Österlund, Elmeri; Suihkonen, Sami; Ross, Glenn; Torkkeli, Altti; Kuisma, Heikki; Paulasto-Kröckel, Mervi

Metalorganic chemical vapor deposition of aluminum nitride on vertical surfaces

Published in:
Journal of Crystal Growth

DOI:
10.1016/j.jcrysgro.2019.125345

Published: 01/02/2020

Document Version
Peer-reviewed accepted author manuscript, also known as Final accepted manuscript or Post-print

Metalorganic chemical vapor deposition of aluminum nitride on vertical surfaces

Elmeri Österlund[a,*], Sami Suihkonen[b], Glenn Ross[a], Altti Torkkeli[c], Heikki Kuisma[c], Mervi Paulasto-Kröckel[a]

[a] *Aalto University, Department of Electrical Engineering and Automation, PO Box 13500, 00076 Aalto, Finland*
[b] *Aalto University, Department of Electronics and Nanoengineering, PO Box 13500, 00076 Aalto, Finland*
[c] *Murata Electronics Oy, Myllynkivenkuja 6, 01621 Vantaa, Finland*

Abstract

Metalorganic chemical vapor deposited (MOCVD) aluminum nitride (AlN) on vertical sidewalls can be used to implement piezoelectric in-plane actuation and sensing in microelectromechanical system (MEMS) sensors. The AlN films should optimally cover conformally the sidewalls and have good crystal quality with *c*-axis oriented microstructure for optimal piezoelectric properties. Previous MOCVD AlN research has focused on using AlN as a buffer layer for other III-nitrides and so far, AlN growth has not been studied on large vertical surfaces. In this study, AlN thin films were grown using MOCVD on vertical sidewalls of fabricated templates and the conformality and crystal quality was characterized. The growth template fabrication was optimized with respect to surface roughness, the conformal coverage was analyzed by measuring the thickness profiles of the films, and the crystal quality was investigated using in-plane XRD and TEM. The AlN films have good crystal quality (FWHM 1.70°–3.44°) and *c*-axis orientation on vertical Si(111) sidewalls. However, the thicknesses of the films reduce approximately at a rate of 0.8–1.2 nm/μm down the sidewall. Lowering the reactor pressure improved the conformal coverage while changing the growth mode from columnar to step-flow, which also improved the film morphology.

Keywords: A3. Metalorganic chemical vapor deposition; B1. Nitrides; B2. Piezoelectric materials; B1. Aluminum nitride

1. Introduction

Piezoelectric actuation and sensing offer several benefits for microelectromechanical (MEMS) devices, such as lower power consumption and higher electromechanical coupling when compared to electrostatic and current-based methods [1]. Wurtzite c-axis oriented aluminum nitride (AlN) is an interesting material for piezoelectric MEMS devices because it has relatively high piezoelectric constants ($d_{33} = 3.4$ pm/V, $e_{31} = 1.0$ C/m^2) and low dielectric permittivity (10.4), giving AlN competitive piezoelectric figures of merit [2]. Furthermore, AlN has good semiconductor process compatibility, high mechanical strength [3] and it is chemically stable [4].

AlN is already used in MEMS devices such as thin film bulk acoustic resonators (FBAR) [5, 6], microphones [7] and piezoelectric micromachined ultrasound transducers (PMUT) [8, 9]. In addition, AlN would be a suitable material for MEMS energy harvesters [10]. AlN is also a promising piezoelectric material for inertial MEMS sensors, such as gyroscopes. The higher electromechanical coupling would, for example, increase the accuracy of the inertial MEMS sensors, which in turn improves inertial navigation.

However, modern three-axis devices require in-plane actuation and sensing, which is challenging to implement with current micromachining methods. So far, the lack of easy in-plane actuation has hindered the integration of piezoelectrics into inertial MEMS sensors. More effective in-plane actuation and sensing can be reached if the piezoelectric elements are fabricated on the vertical sidewalls of the actuator structure. The current method for AlN deposition in MEMS fabrication is reactive sputtering, which is a line-of-sight method and not suited to meet the requirements for conformality and crystal orientation on vertical sidewalls.

Metalorganic chemical vapor deposition (MOCVD) is better suited to meet these requirements [11]. Furthermore, the crystal quality of MOCVD films is generally better compared to sputtered films. MOCVD has been previously used to grow AlN in other fields of technology, such as optoelectronics [12, 13] and RF filters [14]. Generally, CVD methods have better conformality compared to physical vapor deposition (PVD). However, so far MOCVD AlN research has focused on using AlN as a buffer layer for gallium nitride (GaN) [15] and AlGaN and the growth on vertical structures has not been studied. Some experiments have been conducted on epitaxial

*Corresponding author
Email address: elmeri.osterlund@aalto.fi (Elmeri Österlund)

lateral overgrowth of AlN [16, 17] and GaN [18] and selective area growth of GaN [19–21], with the focus of reducing dislocation densities. However, in these studies, the trenches have been shallow, only in the order of few micrometers.

This paper investigates AlN growth on vertical sidewalls, which would enable in-plane piezoelectric actuation and sensing. First, the fabrication of sidewall test structures by potassium hydroxide (KOH) etching of silicon is optimized for AlN growth. Then, the conformality and crystal structure of AlN films grown on the vertical test structures are studied. Additionally, the MOCVD process is studied and optimized on blank Si(111) substrates.

2. Experimental

2.1. Sidewall growth template fabrication

In order to study the conformal coverage and crystal structure of the AlN film on vertical sidewalls, suitable growth templates were developed first. A schematic of the planned template is presented in Fig. 1. Trenches with vertical sidewalls can be etched into (110) silicon wafers with KOH when the trenches are correctly aligned. This results in vertical sidewalls with (111) surfaces, which is coincidentally preferred for c-axis or (0002) oriented growth of crystalline AlN [22].

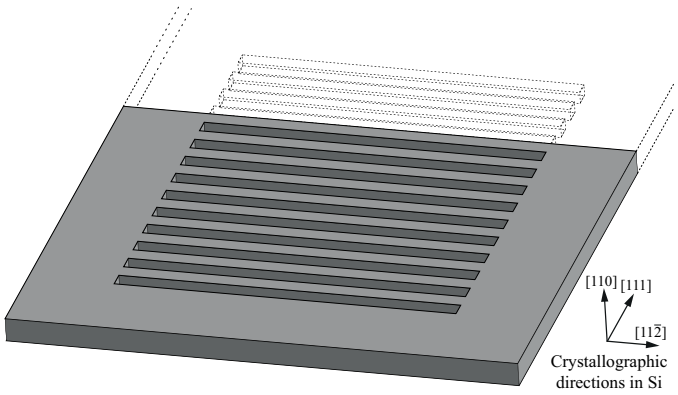

Figure 1: Schematic of the AlN growth template with vertical Si(111) sidewalls fabricated by KOH wet etching of Si(110) wafers.

Before fabricating the growth templates, the KOH etch parameters were optimized, because the surface roughness affects the crystal growth of AlN and the root-mean-square (rms) surface roughness should be in the order of

0.1 nm for good c-axis oriented growth when AlN is sputtered on amorphous Si [23, 24]. Previous studies on KOH etching of Si(110) [25, 26] have not quantitatively analyzed the surface of the etched (111) sidewall or studied it at all. The optimal temperature and KOH concentration in aqueous solution for etched surface quality are in the range of 70 to 80 °C and 40 to 50 % by weight, respectively, according to previous studies.

Before the KOH etching, a SiO_2 hard mask was grown by wet thermal oxidation of Si(110) wafers (4" in diameter and 200 μm thick). The 1 μm thick mask was patterned using photolithography and reactive ion etching. The wafers were then KOH etched for 150 minutes in a temperature-controlled tank at constant KOH concentration.

The surface roughness after etching was analyzed with atomic force microscopy (AFM) and visual inspection was done using scanning electron microscopy (SEM) by dicing etched samples in half along the etched trench and mounting them vertically, as shown in Fig. 2. The rms roughnesses were measured in a NT-MDT Ntegra AFM over a 5 by 5 μm^2 area using a silicon cantilever tip (nominal tip radius 10 nm) in tapping mode. The SEM inspection was done with JEOL JSM-6335F microscope. Vertical and lateral etch rates, as well as the verticality of the sidewalls, were estimated by taking cross-sectional SEM micrographs of the etched samples. The cross-sections were made by mechanical grounding and polishing.

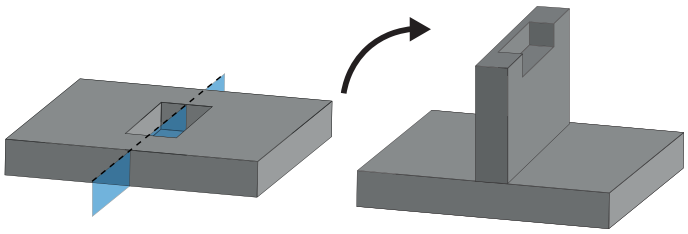

Figure 2: Test samples used in analyzing the etched sidewall roughness. After KOH etching, the samples were diced in half and mounted vertically, giving AFM and SEM access to the etched sidewall.

After finding the optimal KOH etch parameters, the growth templates were fabricated. The template size was 3 by 3 cm^2 and each template had 100 trenches with an aspect ratio of 1, which were nominally 20 mm long, 100 μm wide and deep, and spaced 100 μm apart.

2.2. Metalorganic chemical vapor deposition of AlN thin films

AlN thin films were grown on both the etched templates with vertical sidewalls and on blank Si(111) substrates in a Thomas Swan 3x2" close-coupled showerhead MOCVD reactor. Fig. 3 shows a schematic of the AlN film on the vertical sidewall with the crystallographic orientations.

The growth process began with surface preparation by annealing and nitriding. Annealing was done first at a temperature of 1 065 °C for 5 min under hydrogen (H_2) atmosphere and then for another 5 min under silane (SiH_4) flow at the same temperature. Nitriding was done at a temperature of 1 020 °C under ammonia (NH_3) molar flow of 223 μmol/min for 15 s. After surface preparation, a low-temperature (LT) AlN buffer layer was grown at a temperature of 1 020 °C for 3 min. Trimethylaluminum (TMAl, $Al_2(CH_3)_6$) carried by hydrogen and NH_3 were used as the precursors with flows of 14.59 μmol/min and 110 sccm, respectively, resulting in a V/III ratio of 337. The reactor pressure was 6.67 kPa (50 Torr) in the base process. Finally, the AlN layer was grown at a temperature of 1 125 °C for 25 to 160 min.

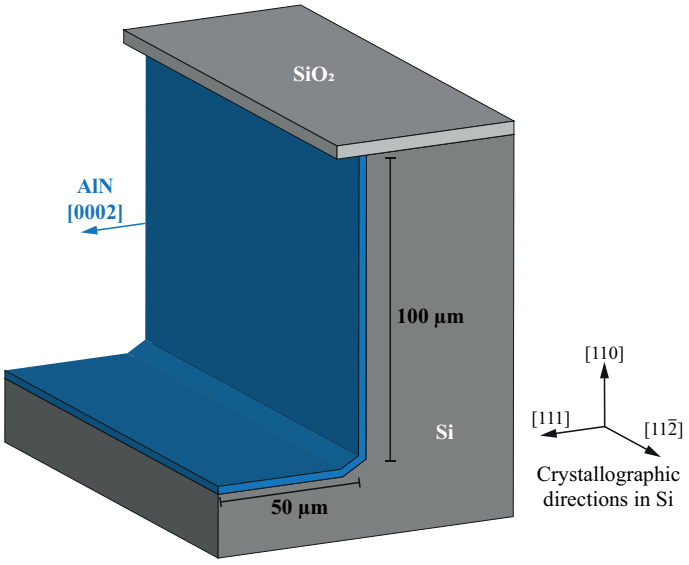

Figure 3: Schematic of an AlN thin film grown on the vertical Si(111) sidewall of an etched trench on the growth template.

In this process, the AlN film should grow only on the vertical (111) sidewalls and on the trench (110) bottom. The remaining SiO_2 hard mask on the top of the substrate should prevent the growth of AlN there. However,

the SiH_4 bake might change this by growing a thin layer of Si on the top as well, on top of which AlN can grow. The purpose of the SiH_4 bake was to homoepitaxially grow some clean Si in order to reduce the effect of possible surface contamination.

Wurtzite AlN tends to grow with the (0002) c planes parallel to the substrate surface, despite the fact that the surface energy of the c planes is higher than the surface energies of the a $(11\bar{2}0)$ and m $(10\bar{1}0)$ planes [27]. For GaN, the presence of hydrogen and nitrogen lower the surface energy of the c planes, making them the most stable plane [28]. Because of the similarities between AlN and GaN, it is plausible that the AlN(0002) planes are the most stable under hydrogen-containing MOCVD conditions as well. This has also been experimentally confirmed in several studies. In summary, it can be assumed that AlN should grow in the (0002) orientation on the vertical sidewalls as well. However, this has not been experimentally studied.

The effect of suspector rotation and reactor pressure on the conformality was studied by using rotation speeds of 5, 30 and 100 rpm and pressures of 20, 35 and 50 Torr. The conformality was evaluated by measuring the thickness profile of the AlN film along the vertical sidewalls. First, the growth templates were cleaved perpendicular to the sidewalls and then cross-sectional SEM micrographs were recorded down the sidewalls at 10 μm intervals in a Zeiss Supra 40 SEM. The thickness of the AlN layer was measured from the micrographs. Thickness and refractive index of the AlN layers on the blank Si(111) substrates was measured using a Philips Plasmos ellipsometer with a wavelength of 632.8 nm.

Because the high growth temperature of 1 125 °C can be considered challenging for process integration the film quality was studied at lower growth temperatures. AlN films were grown on blank Si(111) substrates at temperatures of 750, 875 and 1 000 °C in addition to the base temperature of 1 125 °C.

2.3. X-ray diffraction and atomic force microscopy analysis

High-resolution X-ray diffraction (HRXRD) was used to measure the crystal quality of the AlN films grown on the blank Si(111) substrates. Symmetrical 2θ–ω and ω X-ray rocking curves (XRC) were measured about the 0002 reflection, using a PANanalytical X'Pert Pro diffractometer fitted with a $CuK_{\alpha 1}$ X-ray source, producing a wavelength of 1.540598 Å.

If the AlN films on the vertical Si(111) sidewalls are textured with c-axis orientation as planned, the AlN[0002] direction is parallel to the substrate

surface, and the 0002 reflection cannot be accessed in the conventional 2θ–ω diffractometer configuration. Instead, the crystal quality of AlN on sidewalls was characterized using in-plane XRD. The experimental setup with the in-plane diffractometer angles is presented in Fig. 4. Symmetrical $2\theta_\chi$–ϕ scans and ϕ rocking curves were measured with a Rigaku SmartLab diffractometer. The X-ray source used $\mathrm{CuK}_{\alpha 1}$ radiation as well. Both the θ and ω angles were 0.38°, which yielded maximum reflected intensity.

The measured XRD peaks were fitted using the Lorentzian distribution with the following probability density function $f(2\theta)$

$$f(2\theta) = \frac{A}{\pi\gamma}\left(\frac{\gamma^2}{(2\theta - 2\theta_0)^2 + \gamma^2}\right), \tag{1}$$

where A is a scaling factor, $2\theta_0$ a location parameter and γ a scale parameter. The Lorentzian distribution gives the XRD peak centroids and the full width at half maximums (FWHM) of the peaks as $2\theta_0$ and 2γ, respectively.

The FWHM of the AlN 0002 XRC can be used as an indication of the piezoelectric properties of AlN [29–33]. The results vary somewhat, but once the FWHM of the rocking curve is less than 2°, the AlN film should have reached its full piezoelectric properties.

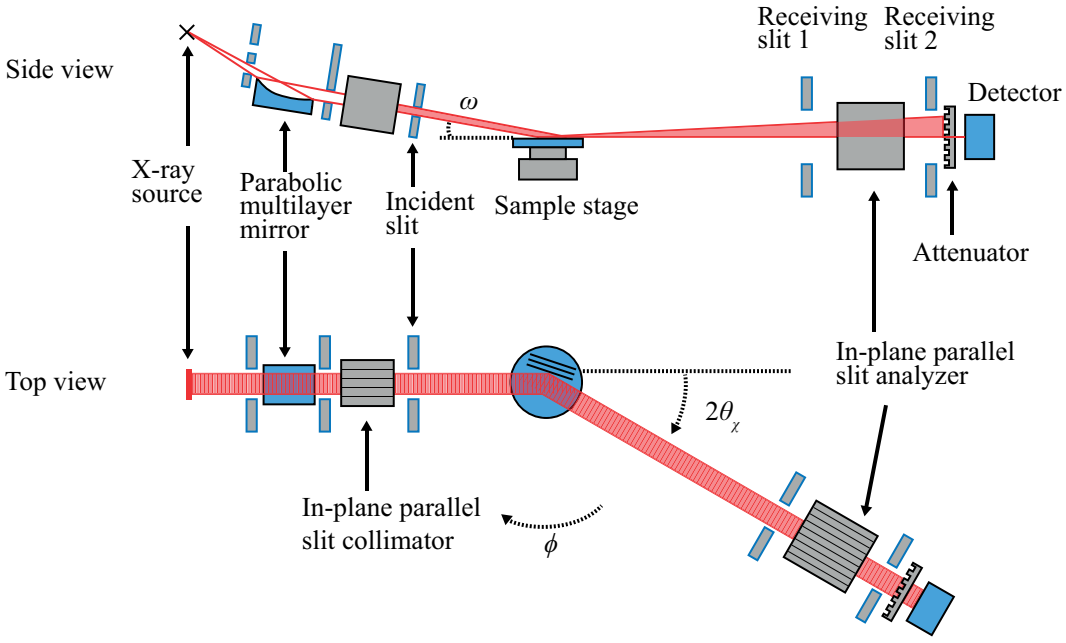

Figure 4: The in-plane XRD measurement setup used for measuring the crystal structure of AlN on the vertical sidewalls. Adapted from [34].

The surface morphologies of the AlN films grown on the blank Si(111) substrates were measured with AFM. A Bruker Dimension Icon AFM in tapping mode was used to measure 5×5 μm^2 areas on the samples. The nominal radius of the silicon AFM tip was 8 nm.

2.4. Transmission electron microscopy and sample preparation

Transmission electron microscopy (TEM) was used to study directly the microstructure of the AlN films and the orientation relationship between the AlN film and the vertical Si(111) sidewalls. First, focused ion beam (FIB) was used to prepare electron transparent lamellas of the AlN films on the vertical sidewalls in an FEI Helios Nanolab 600 dual beam system. Ga-ions were used to mill and polish the cross-sectional lamellas. The lamellas were imaged in a high-resolution JEOL JEM-2800 microscope under 200 kV acceleration voltage. Both bright-field (BF) TEM micrographs and electron diffraction patterns were recorded. The select area electron diffraction patterns (SADP) were recorded along the Si [11$\bar{2}$] zone axis. The prepared lamellas were taken from the top part of the trench.

3. Results and discussion

3.1. KOH etching

Table 1 presents the measured etch rates for Si (110) and (111) planes, selectivity and measured surface roughness at different KOH concentrations by weight and etch temperatures. The rms surface roughness of the etched vertical Si(111) sidewall is an average of five samples.

Two examples of the AFM micrographs are shown in Fig. 5 for samples etched using parameter combinations of 40 wt.% and 70 °C (Fig. 5a), and 45 wt.% and 80 °C (Fig. 5b). The etched surfaces look visually smooth under SEM. However, some terraces and other large imperfections were observed on the sidewalls of all samples.

Table 1: The KOH etching results after 150 minutes of etching.

KOH etch (wt.%)	°C)	(110) etch rate (μm/h)	(111) etch rate (μm/h)	Selectivity Si/SiO_2	Roughness (nm rms)
40	70	48	2	404	2.0 ± 1.4
	75	62	4	265	4.8 ± 3.3
	80	79	6	460	10.7 ± 5.5
45	70	36	0.4	672	6.0 ± 4.2
	80	77	5	412	10.1 ± 3.1
50	70	25	2	318	9.1 ± 3.3
	75	41	2	408	8.8 ± 3.6
	80	46	41	269	1.7 ± 1.1

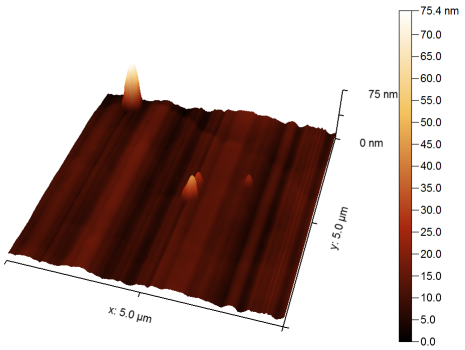

(a) 40 wt.% and 70 °C.

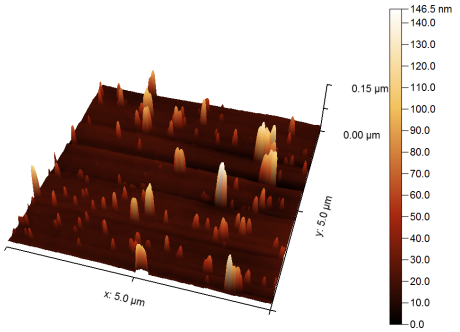

(b) 45 wt.% and 80 °C.

Figure 5: AFM micrographs of the vertical Si(111) sidewall after etching in KOH solution, using KOH etch parameters of (a) 40 wt.% and 70 °C, and (b) 45 wt.% and 80 °C.

Based on the surface roughness and etch rate measurements, the optimal KOH concentration is 40 wt.% at a temperature of 70 °C and these parameters were used to fabricate the vertical Si(111) sidewall templates used as substrates in AlN growth. KOH etch parameters of 50 wt.% and 80 °C were not selected due to high Si(111) etch rate and lower Si to SiO_2 selectivity. Lower etch temperature and concentrations were not investigated due to the slow etch rates.

The measured surface roughness is not well explained by any of the parameters. Although, there is some correlation between the (111) etch rate and the surface roughness: slower (111) etch rate seems to result in smoother etched (111) sidewall. However, there is quite a lot of scattering in the results and the 50 wt.% and 80 °C combination is an outlier. The standard

deviations are also somewhat large in the surface roughness measurements. This could indicate that the roughness is not uniform across the etched sidewall. Another source for the scatter in the data is in the sample fabrication. Dicing of the samples led to generation of Si particles, that were difficult to remove despite protecting the samples with photoresist before dicing and thorough cleaning after. Thus, sample preparation contributes to a part of the measured surface roughness. Based on the previously published results on AlN growth on rough surfaces [23], the achieved rms surface roughness of 2.0 nm might not be smooth enough for the growth of textured and c-axis oriented AlN.

3.2. AlN on blank Si(111) substrates

Table 2 summarizes the growth rate, refractive index, and HRXRD results of AlN grown at different temperatures on the blank Si(111) substrates. The HRXRD 2θ–ω and ω rocking curves are presented in Fig. 6 for the films grown at temperatures of 1 000 and 1 125 °C. With HRXRD, no measurable AlN 0002 reflections were detected for the films grown at lower temperatures. The growth time was 25 minutes, the reactor pressure was 50 Torr and the susceptor rotation speed was 100 rpm.

Using the diffractometer used in the in-plane XRD measurements with a more intense X-ray beam and wider detector acceptance angle, it was possible to observe the 0002 reflections of the AlN films grown at temperatures of 875 and 750 °C. The 0002 peak intensity decreased rapidly with decreasing temperature and the peaks became wider. Moreover, a $10\bar{1}1$ peak emerged in the film grown at a temperature of 875 °C and was clearly observed in the film grown at 750 °C.

Table 2: Growth rate, refractive index, and HRXRD results of AlN films on the blank Si(111) substrates grown at different temperatures. The reactor pressure was 50 Torr and susceptor rotation speed 100 rpm.

Temperature	Growth rate	Refractive	2θ–ω		0002 XRC
(°C)	(nm/min)	index	2θ (°)	FWHM (°)	FWHM (°)
750	3.57 ± 0.02	1.99 ± 0.01			
875	3.51 ± 0.02	2.01 ± 0.01			
1 000	3.54 ± 0.03	2.03 ± 0.01	36.243	0.298	2.773
1 125	3.34 ± 0.04	2.03 ± 0.01	36.178	0.189	1.221

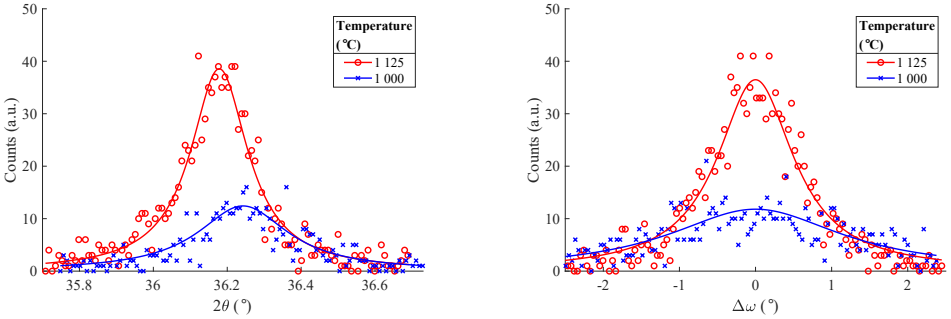

(a) 2θ–ω scans.

(b) ω rocking curves about the 0002 peak maxima.

Figure 6: HRXRD measurements of the AlN 0002 reflection of the films grown at temperatures of 1 000 and 1 125 °C. The AlN films grown at lower temperatures did not produce measurable 0002 reflections in HRXRD. (Only every third measurement point plotted).

The HRXRD results show that the base MOCVD process results in AlN films with high crystal quality and *c*-axis texture, oriented parallel with the Si[111]. However, decreasing the growth temperature reduces the crystal quality sharply. The FWHM of the XRC more than doubles when the temperature is reduced to 1 000 °C and the AlN 0002 peak is significantly less intense. The XRD results show that at a temperature of 875 °C the film starts to lose its texture and at 750 °C the film can be considered almost completely polycrystalline with randomly oriented crystallites. At the same time, the growth rate increases slightly from 3.34 to first 3.54 and finally to 3.57 nm/min. The increase in growth rate is most likely caused by the reduction in the desorption rate of loosely bound atoms at the growth surface [35]. This also explains the reduction in the observed crystal quality, in combination with reduced surface diffusion of precursor molecules due to the lower temperature.

In addition to the change in crystallinity, the surface morphology changed with temperature as well. At 1 125 °C the film surface is grainy and contains a high density of holes. At lower temperatures, the grainy morphology reduced and the surface roughness decreased slightly. Also, the holes mostly disappeared as well. This corresponds well with the observed reduction of crystallinity.

Table 3 shows the evolution of the measured AlN properties as the growth time is increased from 25 minutes to 160 minutes. Figures 7a and 7b show the HRXRD 2θ–ω curves and the ω rocking curves about the AlN 0002 peak maxima, respectively, for the same films.

Table 3: Evolution of AlN film properties on the blank Si(111) substrates as growth time increases. The growth temperature was 1 125 °C, reactor pressure 50 Torr, and susceptor rotation speed 100 rpm.

Time (min)	Thickness (nm)	Refractive index	2θ–ω 2θ (°)	2θ–ω FWHM (°)	0002 XRC FWHM (°)
25	83.4 ± 0.9	2.03 ± 0.01	36.178	0.189	1.221
60	221.4 ± 4.0	1.86 ± 0.02	36.150	0.136	1.207
90	270.3 ± 0.7	2.03 ± 0.02	36.142	0.115	0.963
120	413.1 ± 15.6	1.92 ± 0.05	36.129	0.112	0.840
160	550.5 ± 16.1	2.42 ± 0.20	36.104	0.080	0.632

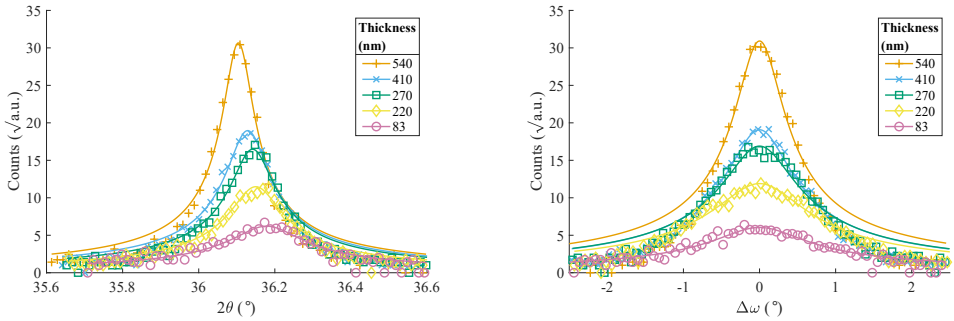

(a) 2θ–ω scans.

(b) ω rocking curves about the 0002 peak maxima.

Figure 7: HRXRD measurements of AlN film of different thicknesses grown on the blank Si(111) substrates. (Only every fifth measurement point plotted.)

Increasing the film thickness increases the AlN crystal quality and the crystallite orientation. The crystal quality increases steadily with the film thickness, as indicated by the decreasing FWHM value of the 2θ–ω 0002 peak, which indicates that the inhomogeneous strain distribution becomes narrower and that the coherence length increases [36]. Furthermore, according to the Scherrer equation the crystallite size increases [37]. The degree of preferential orientation of the AlN crystallites increases as the film thickness increases. The FWHM of the XRC decreases nearly linearly from 1.221° to 0.631°, indicating that the crystallites are better oriented in the same direction.

The AFM results show that as the film thickness increases, the grains continue to grow larger and start to mushroom over the holes, indicating that the columnar grains also grew in size laterally.

In addition to the increasing crystal quality with film thickness, the average residual mechanical stress in the film also seems to decrease. The location of the 0002 peak centroid changes linearly as a function of film thickness from 36.178° to 36.104°. This change corresponds to a change in the lattice constant c from 4.962 Å to 4.971 Å for 83 nm and 550 nm thick films, respectively. This indicates a reduction in the average homogeneous elastic strain of the full film. The out-of-plane elastic strain (ε_c) can be calculated by the following equation

$$\varepsilon_c = \frac{c_{\text{meas}} - c_0}{c_0}, \tag{2}$$

where c_{meas} is the measured lattice constant and c_0 is an unstrained reference lattice constant for AlN [36]. Using 4.98079 Å [38] as the reference value, the strain reduces approximately from -0.38% to -0.20%. The selection of the reference value introduces some error into the calculated strain due to differences in instrumentation and materials.

Assuming that the AlN film is biaxially stressed and very thin compared to the substrate, the biaxial stress σ is given by

$$\sigma = M\varepsilon_a = \frac{E}{1-\nu}\varepsilon_a = -\frac{E}{1-\nu}\frac{1-\nu}{2\nu}\varepsilon_c, \tag{3}$$

where M is the biaxial modulus, ε_a the in-plane elastic strain, E the in-plane Young's modulus and ν the Poisson ratio [39]. Assuming an in-plane Young's modulus of 346 GPa [3] and a Poisson ratio of 0.207 [40], the corresponding in-plane stress reduces from 3.19 GPa to 1.68 GPa.

The residual mechanical stress has two main sources. The first source is the mismatch in thermal expansion coefficients (CTE) between AlN and Si, which induces mechanical stress into the film as it cools down from the growth temperature to the room temperature. The second source is in the difference between the lattice constants of the film and substrate. The most likely explanation for the observed reduction of residual stress is the formation of misfit dislocations, which accommodate the lattice misfit [39]. As the film thickness increases, the total strain energy in the film also increases until it is energetically favorable to generate dislocations. The dislocations accommodate the strain induced by the lattice mismatch between the substrate and the AlN film.

Despite the reducing residual stress, a network of fractures was observed at the surface of the 550 nm thick AlN film. The increasing number of dislocations in combination with the increasing AlN crystallite size reduces the

fracture strength of the film as more dislocations can pile-up into longer pre-cracks within the crystallites [41]. As a result, the remaining residual stress is enough to cause fractures once the fracture strength has been sufficiently reduced.

The results for films grown using reactor pressures of 20 and 50 Torr are summarized in Table 4. Besides the AlN 0002 reflection, no other peaks were detected from the background noise. The growth time was 60 minutes and susceptor rotation speed was 5 rpm.

Table 4: Results of AlN films grown at different reactor pressures on the blank Si(111) substrates. The growth temperature was 1 125 °C and susceptor rotation speed 5 rpm.

Pressure (Torr)	Growth rate (nm/min)	Refractive index	2θ–ω		0002 XRC
			2θ (°)	FWHM (°)	FWHM (°)
20	3.74 ± 0.06	2.03 ± 0.02	36.131	0.063	0.554
50	3.32 ± 0.07	2.07 ± 0.01	36.134	0.062	0.501

Changing the reactor pressure does not seem to affect the crystal quality. Both the XRD peak widths and the intensities remained approximately constant. On the other hand, the film morphology changes at a pressure of 35 Torr. Atomic steps are visible on the surfaces of the films grown at of 20 and 35 Torr, as seen in the AFM micrographs in Fig. 8. This indicates that the film growth mode changes to the step-flow mode from the more common columnar-growth mode. The surface diffusivity of the adsorbed precursor atoms increases at lower pressures [12, 13], which leads to the step-flow growth in this case. The change in the growth mode also leads to a reduction of the observed holes on the film surface. The growth rate increases at lower pressures as well.

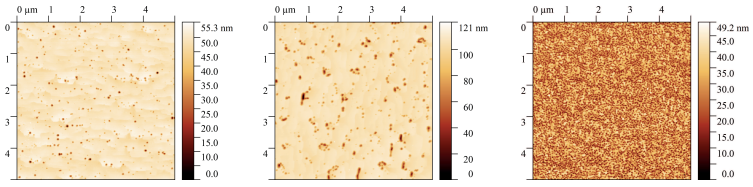

(a) 20 Torr. (b) 35 Torr. (c) 50 Torr.

Figure 8: AFM micrographs of AlN thin films grown at pressures of (a) 20, (b) 35 and (c) 50 Torr on blank Si(111).

3.3. Conformality and crystal quality of AlN on vertical Si(111) sidewalls

The measured profiles of the AlN film thicknesses on vertical sidewalls after 60 min of growth are presented in Fig. 9 using different reactor pressures (Fig. 9a) and susceptor rotation speeds (Fig. 9b). The slope of the profile was used to quantify the conformality and the slope was calculated by fitting a first-degree polynomial line through the measurement points in a least squares sense. The calculated slope tells how much the film thickness reduces in nanometers per one micrometer down the sidewall and they are presented in Table 5.

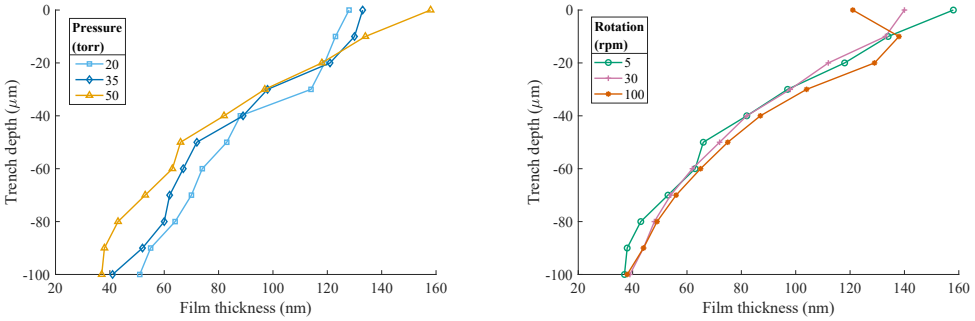

(a) Reactor pressures of 20, 35 and 50 Torr at 5 rpm rotation.

(b) Susceptor rotation speeds of 5, 30 and 100 rpm at a pressure of 50 Torr.

Figure 9: Thickness of AlN films grown on vertical sidewalls as a function of depth, using (a) different reactor pressures and (b) different susceptor rotation speeds. The growth temperature was 1 125 °C.

Table 5: The conformal coverage of AlN films grown on the vertical Si(111) sidewalls at different reactor pressures and susceptor rotation speeds. The closer the slope is to zero, the better.

Pressure (Torr)	Rotation (rpm)	Slope (nm/μm)
20	5	0.84
	30	0.73
	100	0.81
35	5	0.95
50	5	1.20
	30	1.06
	100	1.04

The film morphology changed down the sidewall, as shown by the montage of SEM micrographs in Fig. 10. The montage shows the surface of AlN films grown at pressures of 20 and 50 Torr, at trench depths of 0, 25, 50, 75 and 100 μm. Similar behavior was observed in the AFM measurements as well when film thickness or reactor pressure changed.

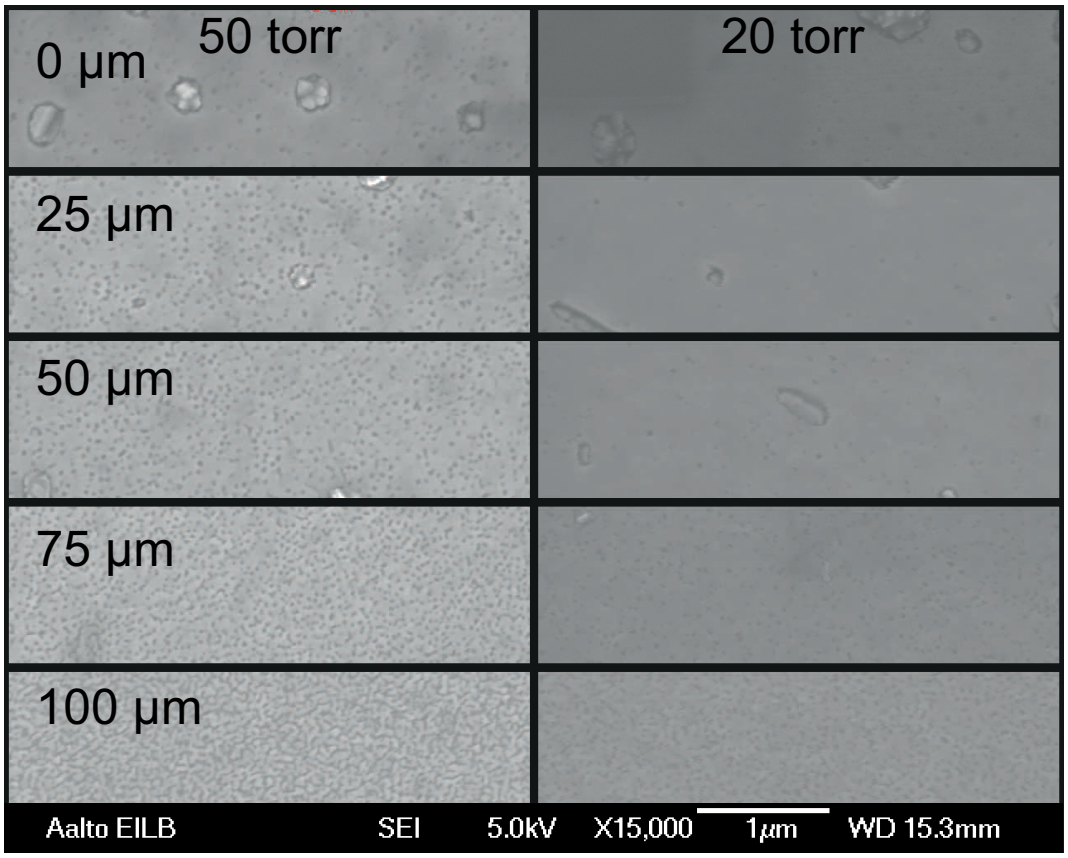

Figure 10: A montage of SEM micrographs of the surface of AlN film grown at 20 and 50 Torr pressures at depths of 0, 25, 50, 75 and 100 μm. The film thickness at each location was shown in Fig. 9a.

The conformal coverage does not seem to change with the used susceptor rotation speed. The results show that the gradient of the film thickness remains approximately constant. In theory, the rotation speed affects the flow of the precursors on the substrate surface. This could possibly affect the transport of precursors to the bottom of the etched trenches and change the conformal coverage. However, according to the results, this does not seem to be the case.

The effect of reactor pressure seems to be negligible as well. Although the film thickness is improved at the lower half of the sidewall at lower pressure, the thickness gradient remains severe. The film morphology, on the other hand, looks quite different between reactor pressures of 20 and 50 Torr. At 20 Torr, the density of holes is less at the bottom of the trench and the film looks continuous all along the sidewall. Whereas at 50 Torr the film still looks like individual islands that are coalescing together to form a continuous film. The improvement of the film conformal coverage and surface morphology as function on reactor pressure can be attributed to the increased diffusivity of the Al source molecule [12, 13]. In addition to reducing the pressure, the Al diffusivity can be increased by increasing the growth temperature. Unfortunately, at 1 125 °C and 20 Torr, the used MOCVD reactor is already at its operational limits. Thus, further experiments were not possible.

While the gradient in the film thickness is not ideal, it should not be an issue for a transverse piezoelectric actuator that is used to excite the vibrational resonant mode of a silicon cantilever at a constant voltage. The force F_{piezo} that the piezoelectric element exerts on the cantilever depends only on the transverse piezoelectric coefficient e_{31} and width (or in this case the depth) of the element h according to

$$F_{\text{piezo}} = e_{31} h v, \tag{4}$$

where v is the drive voltage over the element [42]. The increasing electrical field at a constant voltage as the thickness decreases compensates for the decrease in the end cross-sectional area of the piezoelectric field. Thus, the exerted force does not depend on the film thickness.

The main issue with the thickness gradient is that a dielectric breakdown in the thin portion of the film limits the maximum drive voltage. Furthermore, the worse film morphology at 50 Torr might reduce the dielectric strength of the film or even cause shorts. Thus, reactor pressure of 20 Torr is preferred over 50 Torr. The added benefit of a piezoelectric actuator integrated onto a vertical sidewall is shown by Eq. 4. The transduction factor can be increased by increasing the depth h of the sidewall without increasing the footprint of the structure on the chip.

The in-plane XRD results for AlN films grown on the vertical Si(111) sidewalls are summarized in Table 6. The in-plane XRD measurements are shown in Fig. 11. This time the AlN $10\bar{1}0$ and $10\bar{1}1$ peaks were observed in addition to the 0002 reflection. However, no measurable rocking curves

were detected for them. The effective film thicknesses were approximately 120–160 nm (Fig. 9) for the in-plane XRD measurements.

Table 6: The in-plane XRD results of AlN films grown on vertical Si(111) sidewalls.

Pressure (Torr)	Rotation (rpm)	$2\theta_\chi$–ϕ $2\theta_\chi$ (°)	$2\theta_\chi$–ϕ FWHM (°)	0002 XRC FWHM (°)
20	5	36.10	0.55	3.44
	100	36.07	0.67	2.62
50	5	36.12	0.62	1.70
	30	36.06	0.77	2.44

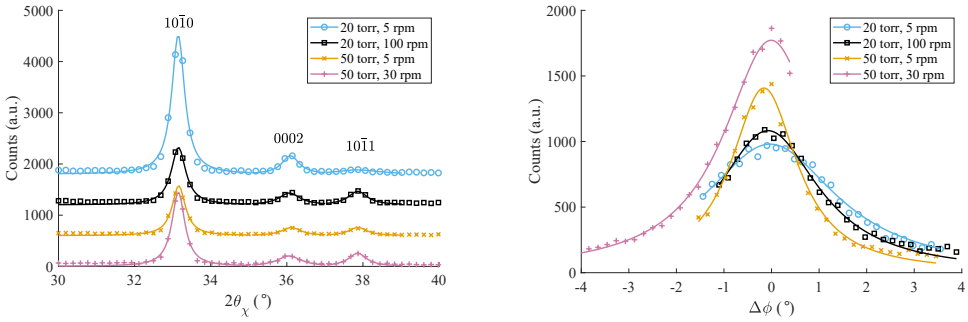

(a) $2\theta_\chi$–ϕ scans.

(b) ϕ rocking curves about the 0002 peak maxima.

Figure 11: The in-plane XRD results of AlN films grown on vertical Si(111) sidewalls. (Only every sixth measurement point plotted.)

The location of the measured ϕ rocking curve maxima differed from the expected 18.05°. The difference was most likely caused by misalignment between the sample and ϕ. Due to the unconventional measurement setup, it was not possible to accurately align the samples so that the etched sidewalls were perfectly parallel with the beam and this caused some offset in the diffractometer ϕ angle. In Fig. 11b instead of plotting the reflected intensity as a function of absolute ϕ angle, the intensities are plotted as a function of $\Delta\phi$, difference from the peak maxima.

At first glance, the crystal quality of the AlN film grown on vertical sidewalls seems to be worse compared to AlN grown on the blank substrates. The in-plane XRD results show that the AlN 0002 reflection peak is rather weak and wide. Moreover, $10\bar{1}0$ and $10\bar{1}1$ reflections are also observed, which would indicate that the AlN film has lost its texture.

However, layers of polycrystalline AlN are observed growing on top of the SiO_2 hard masks as well. A TEM micrograph of a FIB-milled cross-sectional lamella of an AlN film grown at 50 Torr is presented in Fig. 12 for example. AlN grew on top of the SiO_2 layer at lower pressures as well. The observed layer produces the $10\bar{1}0$ and $10\bar{1}1$ reflections in in-plane XRD. This is further confirmed by the in-plane XRD rocking curves. No rocking curves were observed about the $10\bar{1}0$ or $10\bar{1}1$, while curves were successfully measured about the 0002 reflection. The latter can be only produced if the AlN film on the vertical sidewall is textured and c-axis oriented.

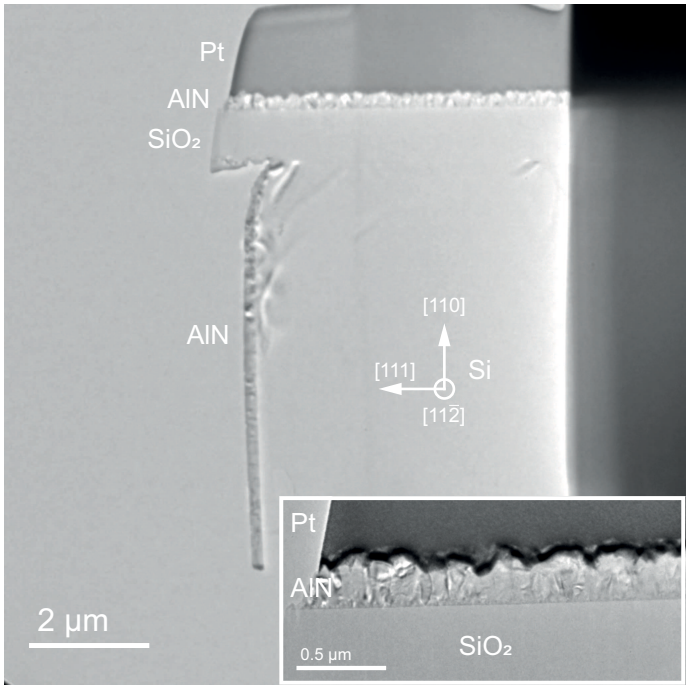

Figure 12: A FIB-milled TEM lamella of an AlN film grown at 50 Torr, showing that in addition to AlN growing on the vertical Si(111) sidewall, it has also grown on top of the SiO_2 layer used as a hard mask for the KOH etching. Inset: The AlN layer on top of SiO_2.

Fig. 13 shows an HRTEM micrograph of the interface between the Si(111) sidewall and AlN. The lattice fringes in Fig. 13 correspond to the AlN(0002) lattice planes and they were observed throughout the thickness of the film. Silicon lattice fringes are not observed at the AlN–Si interface in Fig. 13 most likely due to ion beam induced damage. AlN and Si were ion milled at different rates, thus once the AlN layer was sufficiently thin, the

silicon especially at the interface was already extremely thin and damaged.

A recorded SADP is presented in Fig. 14. The pattern shows diffraction spots for Si with a zone axis of $[11\bar{2}]$ (red crosses) and textured AlN, with the orientation relationship AlN(0002)‖Si(111) AlN$[11\bar{2}0]$‖Si$[\bar{2}20]$. Measuring from the diffraction pattern, the AlN lattice constants were $a = 3.11$ Å and $c = 4.97$ Å. The reciprocal distance was calibrated using the Si(111) diffraction spot and lattice constant of 5.431 Å for Si.

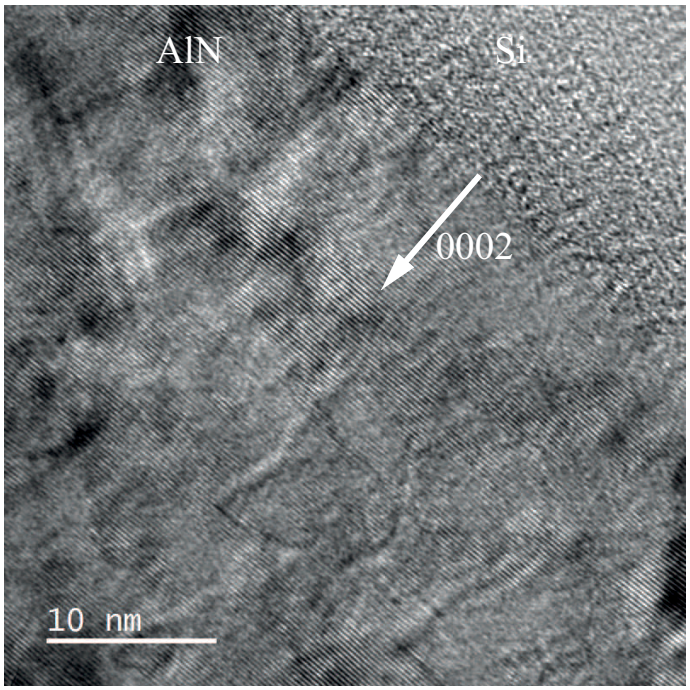

Figure 13: HRTEM micrograph of an AlN film at the AlN–Si interface, grown at 20 Torr on vertical Si(111) sidewall.

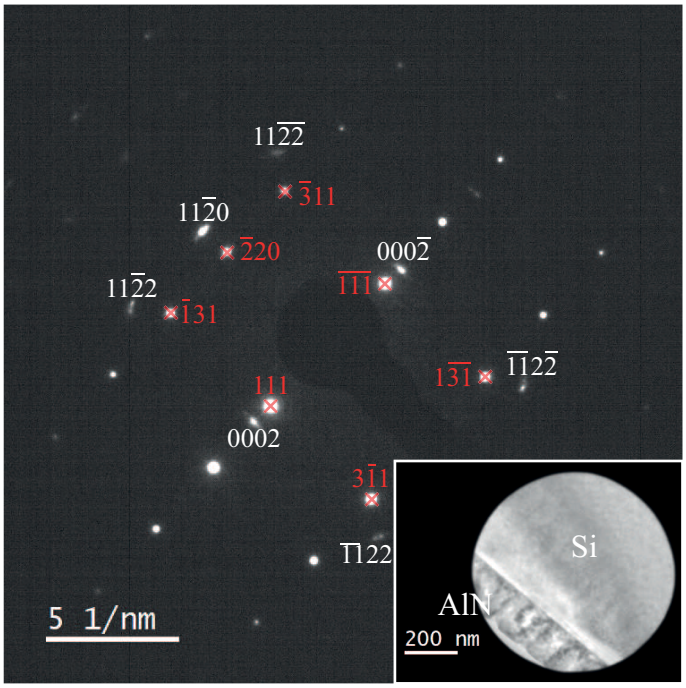

Figure 14: Select area diffraction pattern of the AlN film on Si(111) sidewall, with AlN diffraction spots labedded in white and Si spots in red. Inset: Area where the SADP was recorded from.

The TEM analysis of the films also confirms the texturing of the AlN film. The *c*-axis orientation is maintained throughout the film from the Si–AlN interface to the surface. No differently oriented crystallites were observed. A layer of native aluminum oxide seems to have formed on top of the AlN layer. Even though the Si sidewall surface was rough (Table 1) after etching, the LT-AlN buffer layer has accommodated the surface roughness and the AlN layer has a global orientation, instead of local. The texture and orientation are further confirmed by the recorded electron diffraction patterns.

According to the in-plane X-ray rocking curves, the crystal quality of the AlN films on vertical sidewalls seems to be better when grown at 50 Torr compared to 20 Torr. This is not consistent with the HRXRD result for AlN on blank Si substrates, which showed the crystal quality to remain constant at the tested reactor pressures. Moreover, previously the crystal quality has been shown to improve by reducing the pressure [12]. As there was no noticeable difference in the TEM micrographs or SAD patterns between AlN films grown at 20 and 50 Torr, the observed difference in the crystal

quality in the XRC measurements (Fig. 11b) is likely due to experimental errors of the in-plane XRD measurements. There are two major sources of error unique to this experiment. First, it was not possible to accurately align the sample and ϕ angle, as previously mentioned. Second, the beam diffracted by the (0002) planes is actually reflected inside the sample at an angle of $-\omega$, while the detector was at an angle of ω for the measurement, and instead of measuring the maxima of the XRD peaks, part of the peak tail was measured.

4. Conclusion

In this paper, the growth of AlN by MOCVD on vertical sidewalls was studied as a possible way to implement in-plane actuation and sensing for piezoelectric MEMS sensors. First, the fabrication of Si growth templates with vertical (111) sidewalls using KOH wet etching of Si(110) substrates were optimized with respect to the sidewall surface quality. It was found that a KOH concentration of 40 wt.% and temperature of 70 °C yielded the lowest surface roughness. The rms surface roughness of the sidewall was 2.0 ± 1.3 nm and would have likely been too high for growth of textured high crystal quality AlN. This was overcome by a low-temperature AlN buffer layer that accommodated the surface roughness.

After optimizing the KOH etching, the AlN MOCVD process was studied in more detail on blank Si(111) substrates. The base process parameters for temperature, reactor pressure and susceptor rotation speed of 1 125 °C, 50 Torr, and 100 rpm, respectively, resulted in high-quality crystalline AlN films with *c*-axis orientation, which is the preferred orientation for piezoelectric applications. The growth temperature could not be lowered without a significant loss of crystal quality and orientation. The reactor pressure or susceptor rotation speed did not have a measurable effect on the crystal quality. However, changing the pressure from 50 Torr to 35 Torr changed the growth mode from columnar-growth to step-flow mode, which improved the film morphology. The growth remained in the step-flow mode at a pressure of 20 Torr as well. The film quality increased as a function of the AlN film thickness. The FWHM of the 0002 XRC decreased nearly linearly from 1.221° to 0.632° when the film thickness increased from 83 nm to 550 nm. At the same time, the film residual stress was relieved from 3.19 GPa to 1.68 GPa by the formation of misfit dislocations. However, the increasing crystallite size and dislocation count lowered the fracture strength of the film

with thickness and the residual stress fractured the 550 nm thick film. The high residual stresses are a challenge for reliability and device integration.

Finally, AlN was grown on the vertical Si(111) sidewalls of trenches etched into Si(110) substrates, with an aspect ratio of 1. The in-plane XRD and TEM results show that the AlN film retains it crystal quality and c-axis texture on vertical sidewalls, as is required for in-plane actuation and sensing. The film thickness changes down the etched sidewall and does not cover it conformally. At the top of the sidewall, near the substrate surface, the thickness of the AlN film is approximately 140 nm after 60 minutes of growth. The film thickness gradient is approximately 1.04 nm per 1 μm down the sidewall, thus, at the bottom of the trench at -100 μm, the film thickness is approximately 40 nm. The conformal coverage does not improve at susceptor rotation speeds of 30 or 5 rpm. Reducing the reactor pressure from 50 Torr improves the conformal coverage slightly. At 20 Torr, the gradient is approximately 0.8 nm/μm and the continuity and morphology of the film were improved at 20 Torr as well.

Presently, the crystal quality of AlN grown on vertical sidewalls for in-plane actuation and sensing is sufficient for good piezoelectric properties. While the conformal coverage is not perfect, it is acceptable for transverse piezoelectric actuation. Improving the conformality would most likely require even higher growth temperatures and lower reactor pressures. The effect of aspect ratio should be studied on the conformality as well.

Acknowledgments

Mr. Österlund appreciates the funding from the European Space Agency (NPI grant 4000116390), Aalto ELEC Doctoral School and Murata Electronics Oy. The authors would like to thank: Dr. Ulla Vainio for her help with the in-plane XRD measurements, and Dr. Lauri Riuttanen and Mr. Jori Lemettinen for their help with MOCVD processing. Okmetic Oy is acknowledged for providing the silicon wafers. This research was performed at the Aalto University OtaNano – Micronova Nanofabrication Centre and Nanomicroscopy Center.

References

[1] S. Trolier-McKinstry, P. Muralt, Thin film piezoelectrics for MEMS, J. Electroceram. 12 (1-2) (2004) 7–17 (2004).

[2] M.-A. Dubois, P. Muralt, Properties of aluminum nitride thin films for piezoelectric transducers and microwave filter applications, Appl. Phys. Lett. 74 (20) (1999) 3032–3034 (1999).
[3] E. Österlund, J. Kinnunen, V. Rontu, A. Torkkeli, M. Paulasto-Kröckel, Mechanical properties and reliability of aluminum nitride thin films, J. Alloys Compd. 772 (2019) 306–313 (2019).
[4] D. Zhuang, J. Edgar, Wet etching of GaN, AlN, and SiC: a review, Mater. Sci. Eng. R Rep. 48 (1) (2005) 1–46 (2005).
[5] G. Wingqvist, AlN-based sputter-deposited shear mode thin film bulk acoustic resonator (FBAR) for biosensor applications—A review, Surf. Coat. Technol. 205 (5) (2010) 1279–1286 (2010).
[6] T. Y. Lee, J. T. Song, Detection of carcinoembryonic antigen using AlN FBAR, Thin Solid Films 518 (22) (2010) 6630–6633 (2010).
[7] M. D. Williams, B. A. Griffin, T. N. Reagan, J. R. Underbrink, M. Sheplak, An AlN MEMS piezoelectric microphone for aeroacoustic applications, J. Microelectromech. Syst 21 (2) (2012) 270–283 (2012).
[8] S. Akhbari, F. Sammoura, S. Shelton, C. Yang, D. Horsley, L. Lin, Highly responsive curved aluminum nitride pMUT, in: IEEE 27th Int. Conf. MEMS, IEEE, 2014, pp. 124–127 (2014).
[9] D. Gong, H. Cai, Y. Xia, S. Ma, H. Liu, Y. Chiu, Y. Jin, Fabrication and characterization of AlN based piezoelectric micromachined ultrasonic transducer for contact sensing, in: 2018 19th International Conference on Electronic Packaging Technology (ICEPT), IEEE, 2018, pp. 1442–1447 (2018).
[10] C. Fei, X. Liu, B. Zhu, D. Li, X. Yang, Y. Yang, Q. Zhou, AlN piezoelectric thin films for energy harvesting and acoustic devices, Nano Energy (2018).
[11] A. Yanguas-Gil, Y. Yang, N. Kumar, J. R. Abelson, Highly conformal film growth by chemical vapor deposition. I. A conformal zone diagram based on kinetics, J. Vac. Sci. Technol. A 27 (5) (2009) 1235–1243 (2009).
[12] A. Dadgar, A. Krost, J. Christen, B. Bastek, F. Bertram, A. Krtschil, T. Hempel, J. Bläsing, U. Haboeck, A. Hoffmann, MOVPE growth of high-quality AlN, J. Cryst. Growth 297 (2) (2006) 306–310 (2006).
[13] A. Lobanova, K. Mazaev, R. Talalaev, M. Leys, S. Boeykens, K. Cheng, S. Degroote, Effect of V/III ratio in AlN and AlGaN MOVPE, J. Cryst. Growth 287 (2) (2006) 601–604 (2006).
[14] R. Vetury, M. D. Hodge, J. B. Shealy, High power, wideband single crystal XBAW technology for sub-6 GHz micro RF filter applications, in: IEEE Int Ultrason Symp, IEEE, 2018, pp. 206–212 (2018).
[15] H. Amano, N. Sawaki, I. Akasaki, Y. Toyoda, Metalorganic vapor phase epitaxial growth of a high quality GaN film using an AlN buffer layer, Appl. Phys. Lett. 48 (5) (1986) 353–355 (1986).
[16] M. Imura, K. Nakano, G. Narita, N. Fujimoto, N. Okada, K. Balakrishnan, M. Iwaya, S. Kamiyama, H. Amano, I. Akasaki, et al., Epitaxial lateral overgrowth of AlN on trench-patterned AlN layers, J. Cryst. Growth 298 (2007) 257–260 (2007).
[17] V. Kueller, A. Knauer, U. Zeimer, M. Kneissl, M. Weyers, Controlled coalescence of MOVPE grown AlN during lateral overgrowth, J. Cryst. Growth 368 (2013) 83–86 (2013).

[18] D. Kapolnek, S. Keller, R. Vetury, R. Underwood, P. Kozodoy, S. Den Baars, U. Mishra, Anisotropic epitaxial lateral growth in GaN selective area epitaxy, Appl. Phys. Lett. 71 (9) (1997) 1204–1206 (1997).

[19] J. C. Gagnon, H. Shen, Y. Yuwen, K. Wang, T. S. Mayer, J. M. Redwing, Heteroepitaxial growth of GaN on vertical Si {110} sidewalls formed on trench-etched Si (001) substrates, J. Cryst. Growth 446 (2016) 1–6 (2016).

[20] B. Kunert, W. Guo, Y. Mols, R. Langer, K. Barla, Integration of III/V heterostructures by selective area growth on Si for nano-and optoelectronics, ECS Trans. 75 (8) (2016) 409–419 (2016).

[21] J. Hartmann, F. Steib, H. Zhou, J. Ledig, L. Nicolai, S. Fündling, T. Schimpke, A. Avramescu, T. Varghese, A. Trampert, et al., Study of 3D-growth conditions for selective area MOVPE of high aspect ratio GaN fins with non-polar vertical sidewalls, J. Cryst. Growth 476 (2017) 90–98 (2017).

[22] J. Zhang, H. Cheng, Y. Chen, A. Uddin, S. Yuan, S. Geng, S. Zhang, Growth of AlN films on Si (100) and Si (111) substrates by reactive magnetron sputtering, Surf. Coat. Technol. 198 (1-3) (2005) 68–73 (2005).

[23] A. Artieda, M. Barbieri, C. S. Sandu, P. Muralt, Effect of substrate roughness on c-oriented AlN thin films, J. Appl. Phys. 105 (2) (2009) 024504 (2009).

[24] L. Huang, Y. Li, W. Wang, X. Li, H. Wang, Z. Zhang, G. Li, et al., Growth of high-quality AlN epitaxial film by optimizing the Si substrate surface, Appl. Surf. Sci. 435 (2018) 163–169 (2018).

[25] A. Lipson, E. M. Yeatman, A 1-D photonic band gap tunable optical filter in (110) silicon, J. Microelectromech. Syst 16 (3) (2007) 521–527 (2007).

[26] S.-S. Yun, D.-H. Jeong, S.-M. Wang, C.-H. Je, M.-L. Lee, G. Hwang, C.-A. Choi, J.-H. Lee, Fabrication of morphological defect-free vertical electrodes using a (110) silicon-on-patterned-insulator process for micromachined capacitive inclinometers, J. Micromech. Microeng. 19 (3) (2009) 035025 (2009).

[27] C. E. Dreyer, A. Janotti, C. G. Van de Walle, Brittle fracture toughnesses of GaN and AlN from first-principles surface-energy calculations, Appl. Phys. Lett. 106 (21) (2015) 212103 (2015).

[28] C. E. Dreyer, A. Janotti, C. G. Van de Walle, Absolute surface energies of polar and nonpolar planes of GaN, Phys. Rev. B 89 (8) (2014) 081305 (2014).

[29] H. Loebl, C. Metzmacher, R. Milsom, P. Lok, F. Van Straten, A. Tuinhout, RF Bulk Acoustic Wave Resonators and Filters, J. Electroceram. 12 (1-2) (2004) 109–118 (2004).

[30] S.-H. Lee, J.-K. Lee, K. H. Yoon, Growth of Highly c-Axis Textured AlN Films on Mo Electrodes for Film Bulk Acoustic Wave Resonators, J. Vac. Sci. Technol. A 21 (1) (2003) 1–5 (2003). doi:http://dx.doi.org/10.1116/1.1521961.
URL http://scitation.aip.org/content/avs/journal/jvsta/21/1/10.1116/1.1521961

[31] R. S. Naik, J. J. Lutsky, R. Reif, C. G. Sodini, A. Becker, L. Fetter, H. Huggins, R. Miller, J. Pastalan, G. Rittenhouse, et al., Measurements of the Bulk, c-Axis Electromechanical Coupling Constant as a Function of AlN Film Quality, IEEE Trans. Ultrason., Ferroelectr., Freq. Control 47 (1) (2000) 292–296 (2000).

[32] J. Bjurstrom, D. Rosen, I. Katardjiev, V. M. Yanchev, I. Petrov, Dependence of the Electromechanical Coupling on the Degree of Orientation of c-Textured Thin AlN

Films, IEEE Trans. Ultrason., Ferroelectr., Freq. Control 51 (10) (2004) 1347–1353 (Oct 2004). doi:10.1109/TUFFC.2004.1350963.

[33] F. Martin, P. Muralt, M.-A. Dubois, A. Pezous, Thickness dependence of the properties of highly c-axis textured AlN thin films, J. Vac. Sci. Technol. A 22 (2) (2004) 361–365 (2004).

[34] S. Kobayashi, X-Ray Thin-Film Measurement Techniques IV. In-Plane Diffraction Measurements, Rigaku Journal 26 (1) (2010).

[35] G. Bauer, W. Richter, Optical characterization of epitaxial semiconductor layers, Springer Science & Business Media, 2012 (2012).

[36] M. Moram, M. Vickers, X-ray diffraction of III-nitrides, Rep. Prog. Phys. 72 (3) (2009) 036502 (2009).

[37] F. T. L. Muniz, M. A. R. Miranda, C. Morilla dos Santos, J. M. Sasaki, The Scherrer equation and the dynamical theory of X-ray diffraction, Acta Crystallogr. A 72 (3) (2016) 385–390 (2016).

[38] D. Nilsson, E. Janzén, A. Kakanakova-Georgieva, Lattice parameters of AlN bulk, homoepitaxial and heteroepitaxial material, J. Phys. D: Appl. Phys. 49 (17) (2016) 175108 (2016).

[39] W. D. Nix, Mechanical properties of thin films, Metall. Trans. A 20 (11) (1989) 2217 (1989).

[40] I. Yonenaga, T. Shima, M. H. Sluiter, Nano-indentation hardness and elastic moduli of bulk single-crystal AlN, Jpn. J. Appl. Phys. 41 (7R) (2002) 4620 (2002).

[41] M. A. Meyers, A. Mishra, D. J. Benson, Mechanical properties of nanocrystalline materials, Prog. Mater Sci. 51 (4) (2006) 427–556 (2006).

[42] V. Kaajakari, et al., Practical MEMS: Design of microsystems, accelerometers, gyroscopes, RF MEMS, optical MEMS, and microfluidic systems, Las Vegas, NV: Small Gear Publishing (2009).